Journal of Materials Chemistry B

Accepted Manuscript

ROYAL SOCIETY OF CHEMISTRY

www.rsc.org/materialsB

Journal Name

RSCPublishing

ARTICLE

Ti-SrO metal matrix composites for bone implant materials

Yu Wang,[a] Cynthia Wong,[a] Cuie Wen,[b] Peter Hodgson [a] and Yuncang Li*[a]

Cite this: DOI: 10.1039/x0xx00000x

Received 00th January 2012,
Accepted 00th January 2012

DOI: 10.1039/x0xx00000x

www.rsc.org/

Titanium-strontia (Ti-SrO) metal matrix composites (MMCs) with 0, 1, 3 and 5% (weight ratio) of SrO have been fabricated through powder metallurgy method. Increasing the weight ratio of SrO from 0 to 5 %, the compressive strength of Ti-SrO MMCs increased from 982 MPa to 1753 MPa, while the ultimate strain decreased from 0.28 to 0.05. The elastic moduli of Ti-3SrO and Ti-5SrO MMCs were higher than those of Ti and Ti-1SrO MMC samples. Additionally, the micro hardness of Ti-SrO MMCs was enhanced from 59% to 190% with the addition of SrO. The enhanced compression strength and micro hardness of Ti-SrO MMCs were attributed to the Hall-Petch effect and the SrO dispersion strengthening in the Ti matrix. MTS assay results demonstrated that Ti-SrO MMCs with 3% SrO exhibited enhanced proliferation of osteoblast-like cells. Alkaline phosphatase activity of cells was not influenced significantly on the surface of Ti-SrO MMCs compared with pure Ti in a term longer than 10 days. The cell morphology on the Ti-SrO MMCs was observed using confocal microscopy and scanning electron microscopy, which confirmed that the Ti-3%SrO MMCs showed the optimal in vitro biocompatibility.

1. Introduction

Titanium (Ti) and Ti alloys are widely used for biomedical applications due to their excellent biocompatibility and outstanding mechanical properties [1, 2]. Oxide dispersion strengthening (ODS) effect was employed to improve the ultimate strength [3], hardness [4, 5] and yield strength [6] of Ti-based metallic matrix composites (Ti MMCs). In order to maintain the biocompatibility, Ti MMCs were strengthened using oxide particulates with excellent biocompatibility such as zirconium dioxide (ZrO_2) and silicon dioxide (SiO_2), and it had been demonstrated that Ti MMCs reinforced with ZrO_2 and SiO_2 exhibited enhanced biocompatibility and compressive strength compared to pure Ti [7]. Ball milling was widely applied to mix different phases of particles to achieve dispersive particles within metal matrix particles, for instance, Y_2O_3 [4] or ZrO_2 [7] within Ti powders. For most practical applications, powder metallurgy method was used for the fabrication of the solid bulk materials from powder mixtures. Ball milling combined with vacuum sintering were extensively used to fabricate Ti MMCs reinforced by oxide particles [6, 7].

Strontium (Sr) has attracted enormous attentions as a beneficial element for potential biomedical applications due to its ability to stimulate new bone formation and inhibit bone resorption [8-10]. It has been shown that taking 2g of strontium ranelate orally for three years increased bone mineral density and reduced vertebral fractures risk [9]. Sr loaded by inorganic materials was also found beneficial for new bone formation. Sr^{2+} could enhance the alkaline phosphatase (ALP) activity and suppress the proliferation of osteoclasts [11]. As the radii of Ca^{2+} (114 pm) and Sr^{2+} (132 pm) are similar, the substitution of Ca by Sr in hydroxyapatite (HA) is researched widely [12, 13]. It was also found that the protein binding with Sr in plasma was in the same sequence of magnitude as that of Ca [10]. Recent studies [11-13] showed that a low dose of strontium in biomaterials could play a beneficial effect on bone healing of biomedical implants, but high dose might have an adverse effect. In vitro biocompatibility test suggested that 15 at% of Sr in HA stimulated the proliferation and attachment of MC3T3-E1 osteoblast cells [12]. TiO_2 nanotubes loaded with strontium also displayed improved biocompatibility and enhanced the precipitation of hydroxyapatite in simulated body fluid (SBF) [14].

However, the proliferation and ALP activity of osteoblast cells were inhibited when Sr content was more than 10 at% in Sr-containing calcium silicate [11]. The HA coatings with higher dose of Sr (>38.9 at%) fabricated by micro arc treatment was observed to suppress the adsorption of calcium [12]. There seemed to be a lack of consensus with regards to the proper content of Sr. This could be due to the different delivery systems and fabrication methods used by the various studies. Qiu et al [15] indicated that 1 at% was the optimal concentration in the calcium polyphosphate scaffolds. The proper concentration of Sr was 10 at% in the HA coating synthesized using a hydrothermal method [14]. In another research about HA [16], the proper concentration of Sr was asserted to be 5 at%, and 10 at% of Sr in HA inhibited the proliferation of cells. Thus far, the optimal concentration of Sr in Ti MMCs for biomedical applications has not been ascertained.

In this study, strontia (SrO) was chosen as the source of elemental strontium to improve the in vitro biocompatibility and enhance the strength of the Ti matrix. Novel Ti-SrO MMCs samples were fabricated using powder metallurgical method. The mechanical properties, microstructures, surface characteristics and in vitro biocompatibility of Ti-SrO MMCs were presented.

2. Experimental

Powder metallurgical method was used to fabricate Ti-SrO MMCs samples. Ti powder (99.7 wt% purity, 45 μm, Atlantic Equipment Engineers, Inc., US) and SrO powder (99.9 wt% purity, Sigma Aldrich, Australia) were mixed using ball milling (PM400, Retsch, Germany) under 152 KPa argon atmosphere for 2 h with a ball to powder ratio of 10:1. In this paper, Ti powders mixed with 0, 1, 3 and 5 % (weight percent, hereafter) of SrO, were referred as Ti, Ti-1SrO, Ti-3SrO and Ti-5SrO, respectively. The mixture was uniaxially pressed into green compacts with a diameter of 13 mm and a thickness of 2 mm at 600 MPa. The green compacts were subsequently sintered at 1100 °C in vacuum (lower than 10^{-3} Pa) for 3 h with a preheating and cooling rate of 20 °C/min.

The microstructures of the Ti-SrO MMCs were observed using optical microscopy (OM, DP70, Olympus, Japan) and scanning electron microscopy (SEM, Supra 55 VP, Zeiss, Germany). The elemental analysis was characterized using energy dispersive X-ray spectrometry (EDX, Oxford, UK). A carbon coating was deposited on samples before EDX observation. Linear intercept method was employed to determine the average grain size of MMCs by randomly measuring 150 grains on optical images. The oxygen contents of as-sintered Ti and Ti-SrO MMCs were determined by glow discharge optical emission spectrometry (GDOES), and three samples were tested per group. An analyzed zone with a diameter of 4 mm was discharged at 700 V and 20 mA. The oxygen content at the depth of 50 μm of fresh polished samples was determined as the oxygen content of the sample. The density of composites was measured using the Archimedes method.

The microhardness was tested using a Vickers hardness tester (Leitz Wetzlar 4065, Germany) with a load of 2.94 N ($HV_{0.3}$) and a dwell time of 10 s. The hardness values were measured from 25 indents on each sample. The compressive strength of the Ti-SrO MMCs were evaluated by compression test from 4 samples per group using an Instron universal tester with video extensometer (Instron 5567, US) at an initial strain rate of 0.005 mm/s at room temperature.

The contact angle was measured using a contact angle tester (KSV Cam 101, Finland). All samples were polished up to 1200 grit grinding papers (Struers, Denmark), and the surface roughness R_a was measured using atomic force microscopy (AFM, Cypher, Asylum Research, USA). R_a of all surfaces was 110 ± 8 nm. All Ti and Ti-SrO MMCs samples were stored in the lab room 24 h in advance to prevent the influence of temperature and humidity. Ultrapure distilled water and ethylene glycol with the drop size of 5 μL was used to measure the contact angle of samples. The surface energy was calculated according to Owens-Wendt (OW) method:

$$(1+\cos\theta)\gamma_L = 2\left(\sqrt{\gamma_L^d\gamma_S^d}+\sqrt{\gamma_L^p\gamma_S^p}\right) \quad (1)$$

$$\gamma_S=\gamma_S^d+\gamma_S^p \quad (2)$$

Where θ is the contact angle between liquid droplets and solid surface; the superscripts d and p are for the dispersive component and polar component, respectively; subscripts L and S represent for liquid and solid. The dispersive component, polar component and surface energy for water are 21.8 mJ/m^2, 51.0 mJ/m^2 and 72.8 mJ/m^2, and for ethylene glycol 29.0 mJ/m^2, 19.0 mJ/m^2 and 48.0 mJ/m^2, respectively [17].

Ti-SrO MMCs samples for cell culture were ultrasoicated in distilled water, ethanol and acetone. This was followed by sterilization in a muffle furnace at 180 °C for 3 h. The samples were placed into each well of a 24-well plate. Osteoblast like cells, SaOS2 (Barwon Biomedical Research, Geelong Hospital, Victoria,

Australia) were seeded onto the surface of Ti-SrO MMCs and pure Ti samples at a density of 1 × 10^4 cells per well (132 mm^2). Cell viability and proliferation, total protein and alkaline phosphatase activity of SaOS2 cells were measured using MTS assay [18] (Pierce™ BCA Protein Assay Kit Thermo Scientific, USA) and ALP Assay Kit (Colorimetric, ABCAM, Sapphire Bioscience Pty Ltd, Australia) according to the manusfacturer's instructions, respectively. The data of ALP activities were expressed as micromoles of p-nitrophenyl phosphate produced per hour per milligram of protein (μmol h^{-1} mg^{-1}) by normalizing to the total protein of SaOS2 cells.

To measure the release of Sr ions, Ti-SrO samples were immersed in the cell culture media with a media to surface area ratio of 0.3 ml/cm^2 and then incubated at 37 °C for 72 h. The fluid was withdrawn and filter-sterilized with a 0.22-μm filter (Falcon, BD Biosciences, San Jose, CA, USA) to obtain the extracts of Ti-SrO samples. The concentration of Sr was measured by inductively coupled plasma mass spectrometry (ICP-MS, Agilent 7700X, US). To investigate the effect of released Sr from Ti-SrO samples on the cell viability, a cell culture test was carried out using the indirect contact method according to an international standard (ISO 10993-5: Biological evaluation of medical devices - Part 5: Tests for in vitro cytotoxicity). Briefly, SaOS2 cells were mixed with media at a cell density of 5 x 10^4 cells/ml. A mixture of 200 μl was transferred into a well of 48-well cell culture plate. The cell culture plate was placed in an incubator at a humidified atmosphere with 5 % CO_2 at 37 °C for 24 h to allow for cell attachment. The medium in each well was then removed and an extracts of 200 μl was added to in each well. After further incubation of the cells for 5 d in the 48-well cell culture plates, MTS assay was used to measure the cell number in each well.

The morphologies of SaOS2 cells were observed using a confocal microscopy (Leica SP5, Leica Microsystems, Germany) and SEM. The SaOS2-seeded samples for confocal microscopy were fixed in 2% paraformaldehyde and permeabilized with 0.2% Triton-X 100 in phosphate-buffered saline (PBS) (Sigma Aldrich, Australia) for 10 min at room temperature. The cell-seeded samples were then incubated with 1% Alexa Fluor 568 phalloidin and 40-6-diamidino-2-phenylindole (Life Technologies, Australia) for 40 min at ambient temperature and washed with PBS threee times. The confocal microscopy observations of the SaOS2 cells were carried out whithin one week after staining. For the SEM observation of the cell morphology, cell-seeded samples were dehydrated in an increasing concentration ehanol from 60 to 100 % for 10 min per concentration. This was followed by chemical drying for 10 min using hexamethyldisilazane (Sigma, Australia). A gold layer with 20 nm thickness was coated on the samples before SEM observation.

Data were analyzed using one-way ANOVA analysis of variance (SPSS 14.0 for Windows, SPSS Inc., Chicago, IL) and the statistical difference was considered to be significant at $p < 0.05$.

3. Results

The SEM images of original Ti powders, SrO powders and ball-milled mixture powders are shown in Fig. 1 (a), (b) and (c), respectively. The sizes of as received titanium and strontium oxide powders were approximately 10 and 1 μm, respectively. After ball milling for 2 h, the Ti and SrO powders were mixed homogeneously as shown in Fig. 1 (c and d), and the average size of the mixed powders was approximately 5 μm.

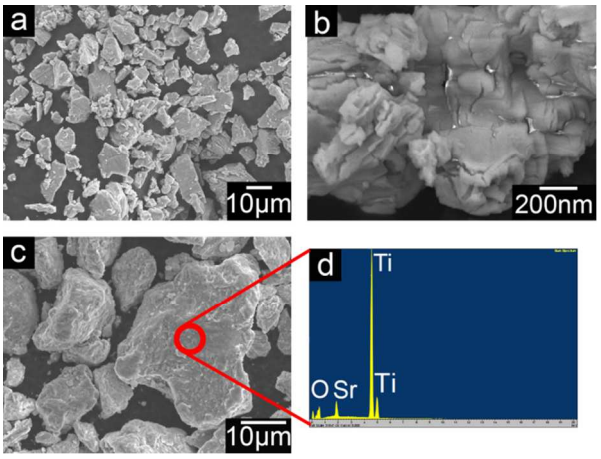

Fig. 1 (a) As-received Ti powders and (b) SrO powders, (c) Ti-5SrO powders and (d) its EDX result after 2h ball milling.

The microstructures of the Ti and Ti-SrO MMCs observed using OM and SEM are shown in Fig. 2. There were more pores in Ti-5SrO MMC compared to Ti-1SrO MMC as shown in the SEM images Fig. 2(k) and (b). Sr was observed in the EDX result (as shown in Fig. 2(l)).

The average grain size and the densities of the Ti-SrO MMCs with different contents of SrO additions are plotted in Fig. 3(a) and (b). The average grain size of the Ti-SrO MMCs decreased gradually with the increase of the SrO content. Titanium without SrO exhibited the largest grain size of 68 μm and Ti-5SrO MMC exhibited the smallest grain size of 20 μm. As shown in Fig. 3 (b), the density of as-sintered pure Ti, Ti-1SrO, Ti-3SrO and Ti-5SrO MMCs were

4.41, 4.39, 4.37 and 4.34 g/cm^3, respectively. The content of oxygen in pure Ti, Ti-1SrO, Ti-3SrO and Ti-5SrO MMCs was 0.24 ± 0.02, 0.29 ± 0.03, 0.34 ± 0.02 and 0.37 ± 0.03 wt%, respectively.

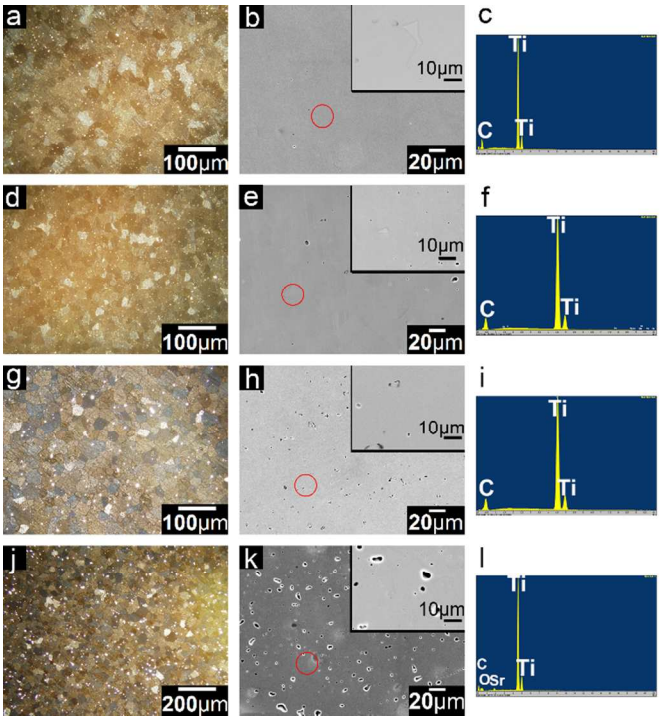

Fig. 2 Optical, SEM micrographs and EDX results of: (a), (b) and (c) Ti; (d), (e) and (f) Ti-1SrO; (g), (h) and (i) Ti-3SrO, (j), (k) and (l) Ti-5SrO MMCs, respectively. The inserted images were SEM micrographs with higher magnification.

Fig. 4 showed the XRD patterns of Ti-SrO MMCs. The weak peaks observed can be attributed to SrO phase (JCPDS: 1-886) in the XRD pattern of the Ti-5SrO MMC. However, no obvious peaks of SrO were detectable in the XRD patterns of the Ti-1SrO and Ti-3SrO MMCs, which was probably due to the minor content of the SrO phase. The main phase of the Ti-SrO MMCs was hexagonal close-packed Ti (JCPDS: 5-682).

The mechanical properties of the Ti-SrO MMCs were tested using compression and hardness test. The compressive strength and the ultimate strain are shown in the Fig. 5(a) and the microhardness in Fig. 5(b). The compressive strength (σ_c) of Ti, Ti-1SrO, Ti-3SrO and Ti-5SrO MMCs were 982, 1335, 1656 and 1753 MPa, respectively. The ultimate strain of pure Ti, Ti-1SrO, Ti-3SrO and Ti-5SrO MMCs were 0.28, 0.20, 0.12 and 0.05. The microhardness of Ti, Ti-1SrO, Ti-3SrO and Ti-5SrO MMCs were 177, 281, 431 and 514 ($HV_{0.3}$), respectively. The elastic modulus of Ti samples was 97.9 GPa, which was similar to the elastic modulus of Ti-1SrO MMC with 98.4 GPa. The elastic moduli of Ti-3SrO and Ti-5SrO were increased significantly to 129.2 and 178.8 GPa, respectively. With the increase in the content of SrO addition, the Ti-SrO MMCs exhibited significant increase in compressive strength and microhardness, but decreased ultimate strain. The standard deviations of the microhardness of the Ti-SrO MMCs were small (2-4%), which suggested that the composite samples were fabricated uniformly using powder metallurgy method.

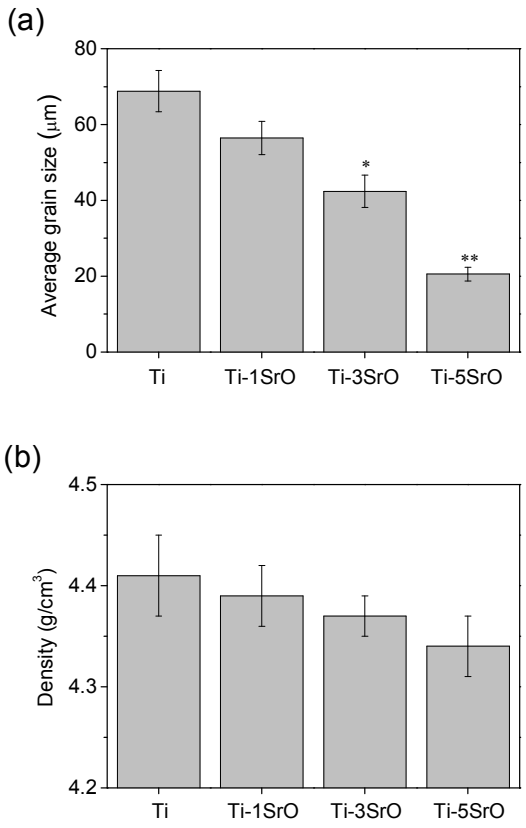

Fig. 3 (a) Average grain sizes and (b) densities of Ti and Ti-SrO MMCs (significantly different from pure Ti samples, *p < 0.05, **p < 0.01, n = 5).

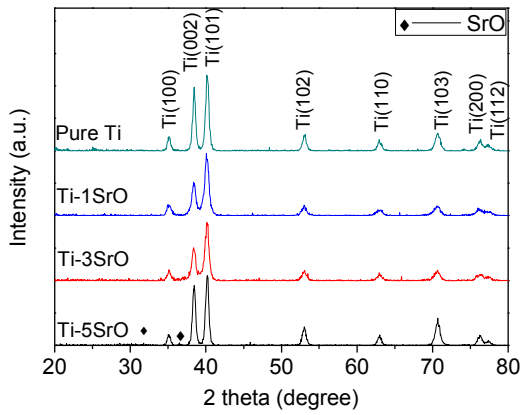

Fig. 4 XRD patterns of Ti and Ti-SrO MMCs.

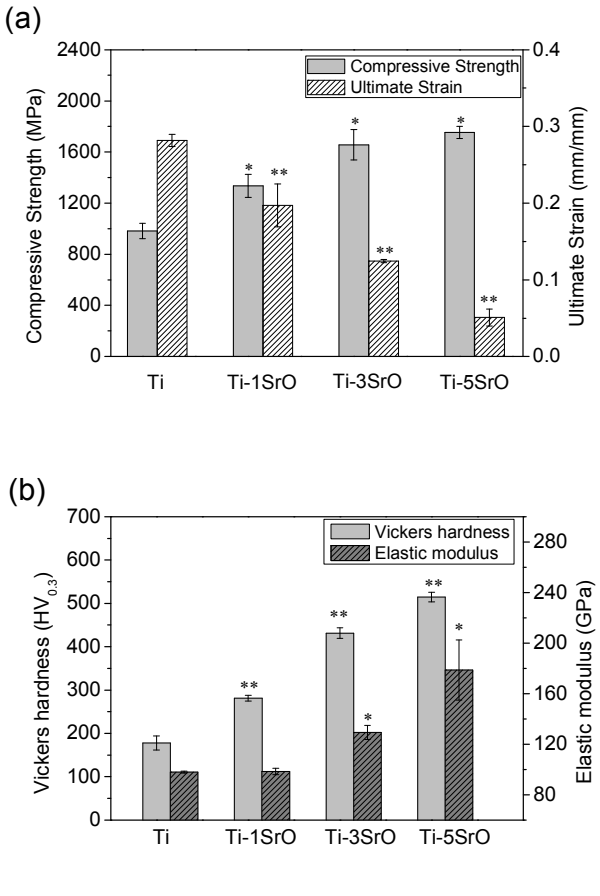

Fig. 5 (a) The compressive strength, ultimate strain and (b) Vicker's hardness and elastic moduli of Ti and Ti-SrO MMCs (significantly different from pure Ti samples, *p < 0.05, **p < 0.01, n=5).

Table 1 shows the contact angle of the Ti-SrO MMCs with distilled water and ethylene glycol droplet and the surface energy calculated using equations (1) and (2). The Ti-SrO MMCs with various content of SrO showed similar hydrophilic properties. The contact angles ranged from 60° to 80° for distilled water, and from 30° to 60° for ethylene glycol. The Ti-SrO MMCs with 5% of SrO showed the greatest hydrophicility and the highest surface energy among all the Ti-SrO MMCs samples. The surface energy of Ti-5SrO MMC was twice that of pure Ti samples.

Table 1 Contact angle with water, ethylene glycol and the surface energy of Ti-SrO MMCs.

	Water (°)	Ethylene Glycol (°)	Surface energy (mJ/m^2)
Pure Ti	66.09(±2.3)	62.11(±0.32)	39.91
Ti-1SrO	76.37(±1.86)	39.074(±4.63)	68.89
Ti-3SrO	70.66(±3.64)	41.1(±6.02)	73.77
Ti-5SrO	60.8(±4.27)	32.16(±4.08)	89.65

Data are shown in the format of mean ± standard error.

Cell proliferation is shown in Fig. 6. After 7 days of culture, there were 2.56×10^5 per disk of SaOS2 cells for pure Ti, 3.22×10^5 for the Ti-1SrO MMC, 4.33×10^5 for the Ti-3SrO MMC, and 3.82×10^5 for the Ti-5SrO MMC. After culturing for 14 days, the number of SaOS2 cells on Ti-1SrO and Ti-3SrO discs were similar to pure Ti, and the Ti-5SrO demonstrated lower cell number than other groups.

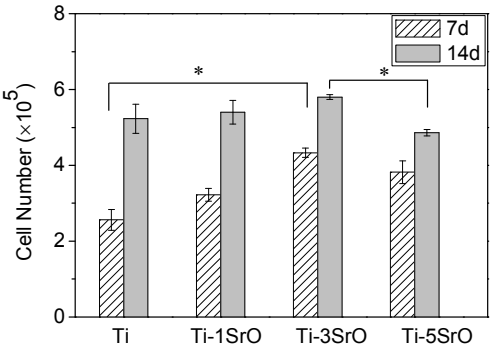

Fig. 6 SaOS2 cell number on the surface of Ti and Ti-SrO MMCs after culturing for 7 and 14 d (*p < 0.05, n=6).

Fig. 7 shows the ALP activities of SaOS2 cells after culturing on pure Ti and Ti-SrO MMCs for 1, 3, 7, 10, 14, 21 and 28. An increase in ALP activity was observed for all four groups, peaking at day 10.

This was then followed by a decrease after Day 14. After 14 days of cell culturing, there was no difference in the ALP activities across the four groups of samples up to day 28. The addition of strontia did not significantly influence the ALP activities of SaOS2 cells on Ti-SrO MMCs.

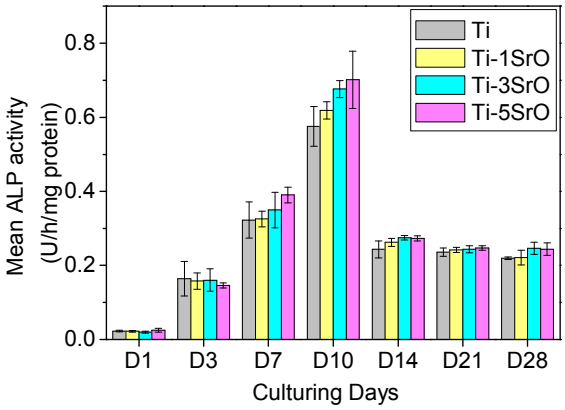

Fig. 7 ALP activity of SaOS2 cells on Ti and Ti-SrO MMCs after culturing for 1, 3, 7, 10, 14, 21 and 28 d.

The morphologies of the SaOS2 cells on the Ti-SrO MMCs on days 1 and 5 were observed using confocal microscopy and SEM, and the images were shown in Fig. 8 and 9, respectively. In the confocal images (Fig. 8), SaOS2 cells attached and spread on the Ti-SrO samples after 1 day of culturing. After culturing for 5 days, a flattened morphology of SaOS2 cells exhibited a well-developed focal adhesion on Ti-SrO MMCs. The SEM images of SaOS2 cells on the surface of Ti-SrO MMCs after incubation for 5 days are shown in Fig. 9. Filopodia of SaOS2 cells were observed for all four groups of samples, showing intercellular adhesion and strong attachment with the substrate.

4. Discussion

4.1 Morphologies of ball-milled powder and Ti-SrO MMCs

The size of Ti powders decreased significantly after ball milling as shown in Fig. 1. Cold welding of powders was also observed in the ball-milled powders. In the ball milling process, the argon gas was employed to prevent the oxidation of Ti powders. No detectable peaks corresponding to TiO_2 were observed in the XRD patterns (Fig. 4). Thus, the oxidation of powders was controlled by filling argon in the ball milling jars. The increasing of content of oxygen (Fig. 3 (c)) was mainly attributed to the oxygen in the SrO particles which was the strengthening element to Ti-SrO MMCs.

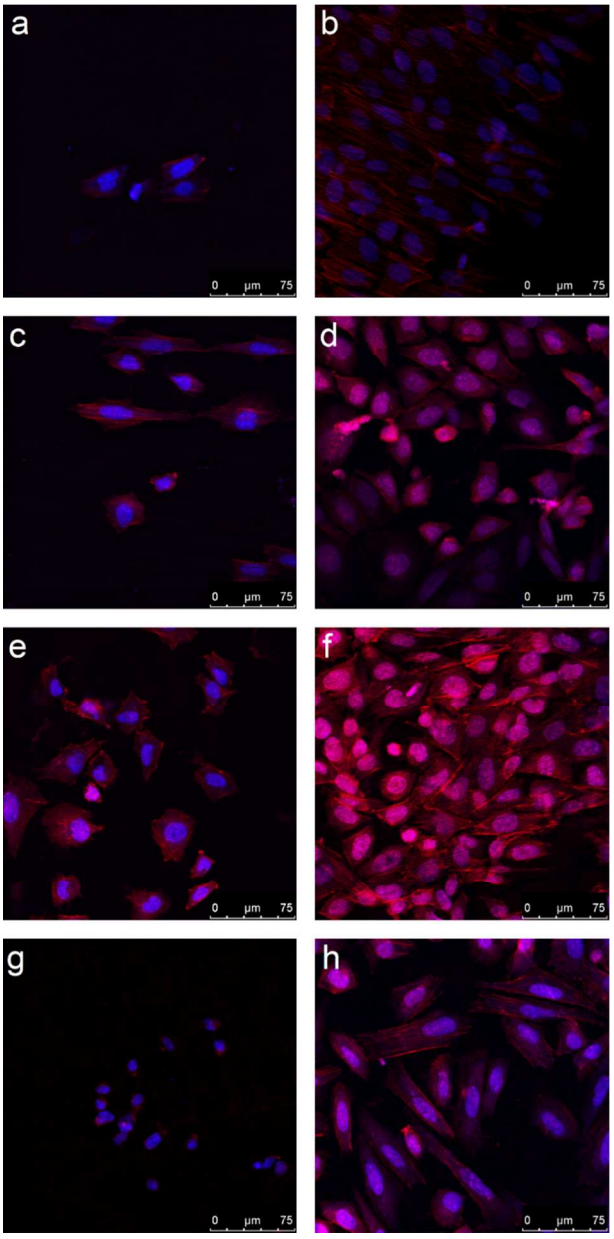

Fig. 8 Confocal images of SaOS2 cells after culturing for 1 and 5 d on: (a) and (b) Ti, (c) and (d) Ti-1SrO, (e) and (f) Ti-3SrO , (g) and (h) Ti-5SrO MMCs, respectively.

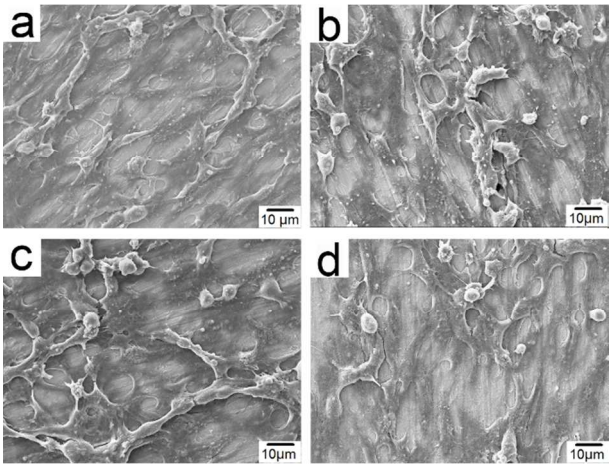

Fig. 9 SEM images of SaOS2 cells after culturing for 5 d on: (a) Ti, (b) Ti-1SrO, (c) Ti-3SrO and (d) Ti-5SrO MMCs.

As shown in Fig. 2, straight grain boundaries were observed in Ti and Ti-SrO MMCs, which confirms the formation of polygonal α-Ti grains. As there was no isostatic pressure was applied during sintering, there were still pores distributed both in grains and between grain boundaries as shown in the optical micrographs of Ti and Ti-SrO MMCs (Figs. 2(a), (d), (g) and (j). The pores in the Ti and Ti-SrO MMC samples exhibited nearly spherical morphologies, which might have a positive effect on the ductility and toughness of the samples [19].

The stability of SrO is dependent on the composition of the alloy, particularly the content of oxygen in the Ti matrix. As the purpose of ball milling in this research was to mix the powders evenly, no alloy was synthesized without long periods of ball milling. The rotation speed was set to 80 rpm to avoid the solid state reactions in the ball milling process. The SrO particles were homogeneously distributed in Ti-SrO MMCs after ball milling and sintering. The Sr was detected in the EDX result after sintering (Fig. 2 (l)), and the weak peak for SrO in the XRD pattern of Ti-5SrO MMC suggested that SrO was the main phase of Sr in Ti-SrO MMCs.

4.2 Improvement of mechanical properties

With the addition of SrO, the compressive strength and microhardness of Ti-SrO MMCs was increased. The elastic moduli of Ti-3SrO and Ti-5SrO MMCs also demonstrated a significant increase. The refinement of grain size of Ti-SrO MMCs is the main reason for the strengthening. The strengthening of grain size is described using Hall-Petch relationship [20], which can be written as:

$$\sigma_{HP} = k/\sqrt{D} \quad (3)$$

where k is the strengthening coefficient and D is the grain size. The as-sintered Ti-SrO MMCs exhibited decreasing grain size with the increase of SrO content. The grain size for pure Ti was 68 μm and 20 μm for Ti-5SrO MMC, leading to the σ_{HP} to increase by 84 % due to Hall-Petch effect.

The addition of oxide acted as pinning point in the Ti matrix [4]. The microhardness increased 2.9 times by adding 5% SrO reinforcement. Krasnowski et al [4] reported that the dispersion of oxide particles in Ti matrix played an important role in the enhancement of hardness of Ti-Y_2O_3 MMCs. Li et al. [7] demonstrated that the compressive strength of Ti-SiO_2 and Ti-ZrO_2 MMCs were dramatically improved by the oxide particles dispersion. One drawback of particulate dispersion was the decline of ultimate strain of the Ti-SrO MMCs as the larger particles tended to stay at the grain boundaries [21], which would impede the motion of grains and increase the stiffness.

In addition, the vacancies had a significant impact on the ultimate compression strength and hardness of substrates strengthened by oxide particles [22]. On one side, porosities improve the hardness of composite samples strengthened by oxide particles [22]. On the other side, higher concentration and larger sizes of vacancies in Ti MMCs strengthened by oxide particles might prevent the migration of Ti grains [3], which might be the main reason for the poor elasticity observed in Ti-5SrO MMC. As shown in Fig.2, increased porosities were produced in Ti-SrO MMCs samples which contained higher addition of SrO. The pores with diameters of about 5 μm in Ti-SrO MMCs were mainly distributed on the grain boundaries (Fig. 2(j)), suggesting that pores might migrate along the grain boundaries during the sintering process.

4.3 Biocompatibilities of Ti-SrO MMCs

The change of surface energy between different Ti-SrO MMC samples was a factor influencing the proliferation of SaOS2 cells. The surface energy of Ti-SrO MMCs increased with the higher addition of SrO contents (as shown in Table 1). The attachment and proliferation of cells to the surface of implants depended on the basic physico-chemical characteristics of material. Higher surface energy of Ti-SrO MMCs is a beneficial factor for the attachment and proliferation of cells. High surface energy enhanced the response of cells to the surface of Ti substrate [23, 24]. The higher surface energy

could influence the local attraction of serum proteins, which ultimately affected the proliferation of cells [23].

There was higher density of cells on the Ti-SrO MMC with 3% SrO addition than pure Ti as shown in Fig. 6. However, increasing the SrO to 5% led to a lower cellular proliferation after 7 days of culturing, which suggested that 5% SrO content in Ti-SrO MMCs repressed the proliferation of SaOS2 cells compared to 3% SrO content.

After immersing samples in cell culture media for 72 h, the concentrations of Sr ions were measured by ICP-MS as 11.6 ± 0.9, 14.4 ± 1.2 and 19.6 ± 1.5 ppb (part per billion) for Ti-1SrO, Ti-3SrO and Ti-5SrO, respectively. The cell number after cell culture for 5 d in the extracts of Ti-1SrO, Ti-3SrO and Ti-5SrO MMCs were 2.08 ± 0.08, 2.18 ± 0.09 and 2.08 ± 0.04 × 10^5, respectively, which showed no significantly difference between them. It indicated that the extracts of Ti-1SrO, Ti-3SrO and Ti-5SrO MMCs had no significant inhibitory effect on cells. Furthermore, the concentrations of Sr released from these composites were far lower than the orally taken strontium ranelate [9, 25]. However, no consensus has been reached as previous in vitro research [26] illustrated that the inhibition effect of Sr was obvious with a concentration higher than 2 ppm. Another study [27] illustrated the in vitro biocompatibility was not affected significantly with 5-20 ppm Sr.

The inhibition effect by high addition of Sr was observed in a study by Lakhkar et al. [28]. When Sr was loaded using hydroxyapatite, Sr at a concentration of 5 at% and higher showed an obvious inhibition effect on cell proliferation. Chung et al. [12] reported that hydroxyapatite coatings with lower Sr addition (10 at%) demonstrated a similar trend to the results in this study, that an appropriate concentration of Sr addition enhanced the bioactivity and biocompatibility of osteoblast cells, and a higher concentration of Sr (>10 at%) inhibited the proliferation of cells.

The addition of strontia to the Ti matrix did not affect the ALP activity of SaOS2 cells significantly. It was shown that the ALP activity for all four groups of Ti-SrO MMCs demonstrated a similar trend, that is, the peak of ALP activity appeared at day 10 and kept stable from day 14 to 28 for all four groups of Ti-SrO samples. The influence of Sr on ALP activity was not observed in other time points. The results of the in vitro assessment indicated that Ti-SrO MMCs were promising biomaterials for tissue engineering according to the performance of cellular proliferation and ALP activity. Another research found that the optimal concentration of SrO was 5 at% in bioglass, and higher concentration of Sr inhibited the ALP activity [26].

Ti-1SrO and Ti-3SrO MMC samples demonstrated excellent in vitro biocompatibility as shown in the confocal micrographs (Fig. 8). Bundles of actin filaments were observed on the Ti-3SrO after 7 d cell culturing. Higher density of SaOS2 cells could be observed on the surface of Ti-3SrO MMC (Fig. 8(f)) compared to Ti-5SrO MMC (Fig. 8(h)). Confocal micrographs suggested that SaOS2 cells preferred Ti-3SrO than Ti-5SrO MMC, which was consistent with cell viability result. SEM images (Fig. 9) demonstrated typical morphology of healthy osteoblast-like cells on Ti-SrO MMCs as well as on pure Ti samples. The enhanced cell proliferation was most likely due to changes in surface energy of the Ti-SrO MMCs with increasing SrO content. It has been shown that SaOS2 cells prefer to attach to surfaces with high surface energy [29, 30]. As shown in Table 1, the surface energy of 3% SrO group was higher than the pure Ti group which correlated to increased cell proliferation in the 3% SrO group when compared to the pure Ti group (Fig. 6). The surface energy was increased with the addition of strontium oxide particles, which was beneficial for the attachment and proliferation of cells.

5. Conclusions

Ti-xSrO (x=0, 1, 3, 5 wt%) MMCs with the addition of SrO nanoparticles were fabricated using powder metallurgy. With the increase in the concentration of SrO, the compressive strength and microhardness of the Ti-SrO MMCs were remarkably enhanced, while the ultimate strain reasonably decreased. The elastic modulus of Ti was similar to Ti-1SrO MMCs, and was remarkably lower than those of Ti-3SrO and Ti-5SrO MMCs. The significant increase in compressive strength and microhardness was attributed to the effects of finer grain size of Ti-SrO MMCs and dispersion strengthening of SrO particles in Ti matrix. In vitro assessment using SaOS2 cells showed that Ti-SrO MMC exhibited enhanced cell proliferation after culturing for 7 and 14 days. In particular, the addition of 3% SrO to Ti matrix displayed the optimal biocompatibility. The ALP activities of SaOS2 cells for all four groups of Ti-SrO MMCs demonstrated that the peak activity occurred at day 10, and remained unchanged from day 14 to 28. Confocal micrographs demonstrated that SaOS2 cells attached and spread healthily on the surface of Ti-SrO MMCs. Combining the influence on the mechanical properties and the in vitro biocompatibility, Ti-3SrO MMC showed the optimal

mechanical and biocompatible behaviours. Further research is needed to clarify the inhibition effect of higher strontium addition (> 5 %) to SaOS2 cells in Ti-SrO MMCs.

Notes and references

[a] Institute for Frontier Materials, Deakin University, Geelong, Victoria 3217, Australia. E-mail: yuncang.li@deakin.edu.au; Fax: +61 352271103; Tel: +61 352272168

[b] Faculty of Science, Engineering and Technology, Swinburne University of Technology, Hawthorn, Victoria 3122, Australia

1. M. Long and H. J. Rack, *Biomaterials*, 1998, **19**, 1621-1639.
2. M. Niinomi, *Metall. and Mater. Trans. A*, 2002, **33**, 477- 486.
3.Y. Liu, Y. Liu, B. Wang, J. Qiu, B. Liu and H. Tang, *Mater. Manuf. Process*, 2010, **25**, 735-739.
4. M. Krasnowski and J. Dąbrowski, *Metall. and Mater. Trans. A*, 2012, **43**, 1376-1381.
5. L. Zhang, S. Ukai, T. Hoshino, S. Hayashi and X. Qu, *Acta Mater.*, 2009, **57**, 3671-3682.
6. T. Yoshimura, T. Thrirujirapaphong, H. Imai and K. Kondoh, *Mater. Sci. Forum*, 2010, **654-656**, 815-818.
7. Y. Li, C. Han, X. Zhu, C. Wen and P. Hodgson, *J. Mater. Sci.*, 2012, **47**, 4410-4414.
8. C. M. Mardiziah, I. Sopyan and S. Ramesh, *Trends in Biomater. and Artif. Organs*, 2009, **23**, 105-113.
9. P. J. Meunier, C. Roux, E. Seeman, S. Ortolani, J. E. Badurski, T. D. Spector, J. Cannata, A. Balogh, E. M. Lemmel, S. Pors-Nielsen, R. Rizzoli, H. K. Genant and J.-Y. Reginster, *New Engl. J. Med.*, 2004, **350**, 459-468.
10. S. P. Nielsen, *Bone*, 2004, **35**: 583-588.
11. W. Zhang, Y. Shen, H. Pan, K. Lin, X. Liu, B. W. Darvell, W. W. Lu, J. Chang, L. Deng, D. Wang and W. Huang, *Acta Biomater.*, 2011, **7**, 800-808.
12. C. J. Chung and H. Y. Long, *Acta Biomater.* , 2011, **7**, 4081-4087.
13. K. C. Kung, T. M. Lee, J. L. Chen and T.-S. Lui, *Surf. Coat. Technol.* , 2010, **205**, 1714-1722.
14. Y. Xin, J. Jiang, K. Huo, T. Hu and P. K. Chu, *ACS Nano*, 2009, **3**, 3228-3234.
15. K. Qiu, X. J. Zhao, C. X. Wan, C. S. Zhao and Y. W. Chen, *Biomaterials*, 2006, **27**, 1277-1286.
16. Y. Fu and D. Chen, *J. Oral Tissue Eng.*., 2005, **2**, 76-80.
17. X. B. Chen, Y. C. Li, P. D. Hodgson and C. E. Wen, *Acta Biomater.* , 2009, **5**, 2290–2302.
18. Y. Wang, C. Wen, P. Hodgson and Y. Li, *J. of Biomed. Mater. Res., Part A*, 2014, **102**, 743-751.
19. R. Roy, D. Agrawal, J. Cheng and S. Gedevanlshvili, *Nature*, 1999, **399**, 668-670.
20. D. G. Morris and M. A. Muñoz-Morris, *Acta Mater.*, 2013, **61**, 4636-4647.
21. L. Carroll, M. Sternitzke and B. Derby, *Acta Mater.*, 1996, **44**, 4543-4552.
22. M. A. Montealegre, M. A. Muñoz-Morris, J. L. González-Carrasco and D. G. Morris, *Scripta Mater.*, 2001, **44**, 2673-2679.
23. G. Zhao, Z. Schwartz, M. Wieland, F. Rupp, J. Geis-Gerstorfer, D. L. Cochran and B. D. Boyan, *J. of Biomed. Mater. Res., Part A*, 2005, **74A**, 49-58.
24. J. Xiong, Y. Li, P. D. Hodgson and C. Wen, *J. of Biomed. Mater. Res., Part A*, 2010, **95A**, 766-773.
25. J.-Y. Reginster, M. Hiligsmann and O. Bruyere, *Ther. Adv. Musculoskelet. Dis.*, 2010, **2**, 133-143.
26. S. Hesaraki, M. Gholami, S. Vazehrad and S. Shahrabi, *Mater. Sci. and Eng., C*, 2010, **30**, 383-390.
27. E. Gentleman, Y. C. Fredholm, G. Jell, N. Lotfibakhshaiesh, M. D. O'Donnell, R. G. Hill and M. M. Stevens, *Biomaterials*, 2010, **31**, 3949-3956
28. N. Lakhkar, E. A. Abou Neel, V. Salih and J. C. Knowles, *J Biomater Appl*, 2011, **25**, 877-893.
29. Y. Li, J. Xiong, C. Wong, P. Hodgson and C. Wen, *Tissue Eng A,* 2009, **15**, 3151-3159.
30. B. Feng, J. Weng, B.C. Yang, J.Y. Chen, J.Z. Zhao, L. He, S.K. Qi, X.D. Zhang, *Mater. Charact.*, 2003, **49**, 129-137.

Ti-SrO metal matrix composites for bone implant materials

Yu Wang,[a] Cynthia Wong,[a] Cuie Wen,[b] Peter Hodgson[a] and Yuncang Li*[a]

Graphic Abstract: